Malaria Journal

RESEARCH

Open Access

Natural triterpenic phenolic esters target PfA-M17 in *Plasmodium falciparum*

Lúcia Mamede[1,2], Gabriel W. Rangel[3], Marjorie Schmitt[4], Sebastien Albrecht[4], Martin Spichty[4], Joanne Bero[1], Claire Beaufay[1], Isabelle Florent[5], Manuel Llinás[3,6], Michel Frédérich[2] and Joëlle Quetin-Leclercq[1*]

Abstract

Background Malaria is a deadly parasitic disease for which innovative treatments are urgently needed. A mixture of eight triterpenic esters (8TTE) was previously identified as important for the antiplasmodial activity of *Keetia leucantha* twigs, a plant used in traditional medicine in Benin. Despite the reported in vitro and in vivo activity, the targets of 8TTE are unknown.

Methods The present study investigated the mode of action of 8TTE on *Plasmodium falciparum* by a multi-scale integrative study from phenotype to metabolome, including: phenotypic analysis, enzymatic tests, molecular docking and metabolomic profiling.

Results This study identified a unique antiplasmodial profile with activity onset in the early-ring stage of the parasite, the inhibition of aminopeptidase PfA-M17 (PlasmoDB PF3D7_1446200) and perturbations in parasite haemoglobin metabolism.

Conclusions Further structure–activity and medicinal chemistry studies are warranted to elaborate on these findings and the potential for 8TTE-related molecules to serve as future antimalarial drugs.

Keywords Malaria, *Plasmodium* spp., Triterpenic esters, Phenotypic analysis, Enzymatic tests, PfA-M17, Molecular docking, Metabolite profiling

Background

Malaria is a parasitic disease caused by *Plasmodium* spp. parasites and is responsible for significant morbidity and mortality across the world [1]. Despite global efforts and intervention strategies, malaria resulted in 263 million cases in 85 malaria-endemic countries and areas in 2023, with tremendous effects on public health [1]. One malaria mitigation strategy is ethnopharmacology, an established field in antimalarial drug discovery (reviewed previously [2]). Indeed, plants traditionally used to treat malaria symptomatology remain important sources of potential antimalarial compounds. However, to transform these plant extracts into lead compounds for antimalarial drug development, extensive knowledge of their mode of action, toxicity, and kinetics is required [3].

Keetia leucantha is a plant traditionally used in Benin for the treatment of malaria through a decoction soup

*Correspondence:
Joëlle Quetin-Leclercq
joelle.leclercq@uclouvain.be
[1] Pharmacognosy Research Group, Louvain Drug Research Institute (LDRI), UCLouvain, Brussels, Belgium
[2] Laboratory of Pharmacognosy, Center of Interdisciplinary Research On Medicines (CIRM), University of Liège, Liège, Belgium
[3] Department of Biochemistry and Molecular Biology and Huck Center for Malaria Research (CMaR), The Pennsylvania State University, University Park, PA, USA
[4] Laboratoire d'Innovation Moléculaire Et Applications (UMR 7042, CNRS—IRJBD, Université de Strasbourg, Université de Haute-Alsace, 3 Bis Rue Alfred Werner, 68057 Mulhouse CEDEX, France
[5] Département Adaptations du Vivant (AVIV), Molécules de Communication et Adaptation des Microorganismes (MCAM, UMR 7245 CNRS), Muséum National d'Histoire Naturelle, CNRS, CP 52, 57 Rue Cuvier, Cedex 05, 75231 Paris, France
[6] Department of Chemistry, The Pennsylvania State University, University Park, PA, USA

taken three times a day [4]. Previous analysis of this plant revealed relevant antiplasmodial activity derived from dichloromethane extracts of twigs and leaves as summarized in Table 1 [5–7]. Bioassay-guided fractionation of the dichloromethane twig extract tested against *Plasmodium falciparum* strain 3D7 in vitro led to the identification of antiplasmodial triterpenic acids (ursolic and oleanolic acids) and eight triterpenic esters (8TTE) shown in Fig. 1 [6]. 8TTE was first obtained as a mixture of four pairs of *E/Z* isomers that showed similar antiplasmodial properties when separated. As their activity and structures are very similar and the *E/Z* isomers transform into each other, the mixture was selected for further tests [4]. 8TTE was tested intraperitoneally at 50 mg/kg/day in vivo in a Peters' 4-day suppressive test in mice infected with *Plasmodium berghei,* and parasitaemia was shown to be significantly (p-value < 0.01) reduced (27.8 ± 5.4%) on day 4 compared to vehicle control [8]. Considering that some pentacyclic terpenes are associated with toxicity, additional tests were conducted in vivo in mice dosed with *K. leucantha* extracts and 8TTE, demonstrating no haemolysis and no acute toxicity up to a cumulative dose of 150 mg/kg [8]. Furthermore, independent ^{1}H-NMR analysis of crude dichloromethane extracts of twigs and leaves of *K. leucantha* showed a correlation between the antiplasmodial activity and the presence of triterpenoids, *i.e.,* the higher the triterpenoid content, the lower the IC_{50} against the parasite, and further identified 8TTE as positively associated with the antiplasmodial activity [9].

In addition to these promising results, understanding the mode of action of 8TTE is crucial to complete its profile as a putative antimalarial. To accomplish this, a multi-omic approach was used, including: phenotypic analysis, enzymatic tests, molecular docking and metabolomic profiling. Phenotypic studies were designed to explore the mode of action of 8TTE on *P. falciparum* 3D7 cultures at different stages of the intraerythrocytic cycle through multiple in vitro assays, which revealed a unique antiplasmodial profile with activity onset in the early-ring stage. Enzymatic assays showed a selective inhibition of rPfA-M17 compared to rPfA-M1 and docking studies indicated a putative interaction between the enzymatic binding sites of recombinant PfA-M1 and PfA-M17 and 8TTE [10]. Finally, metabolomics profiling was performed using 8TTE and several reference antimalarials artemisinin (ART), atovaquone (AVQ) and chloroquine (CQ), revealing that treatment with 8TTE results in perturbations in parasite haemoglobin metabolism [11].

Methods

In vitro culture of *Plasmodium falciparum*

Continuous in vitro cultures of asexual erythrocyte stages of *P. falciparum* CQ-sensitive strain 3D7 were maintained and used in antiplasmodial assays conducted similarly as described elsewhere [12, 13]. Briefly, parasites were cultured in complete medium comprised of RPMI 1640 (Gibco, Fisher Scientific, Loughborough, U.K.) containing sodium bicarbonate (32 mM), HEPES (25 mM), and L-glutamine (300 mg/ml). The medium was supplemented with 1.76 mg/mL of glucose (Sigma-Aldrich, Machelen, Belgium), 44 mg/mL of hypoxanthine (Sigma-Aldrich, Machelen, Belgium), 100 mg/L of gentamycin (Gibco, Fisher Scientific, Loughborough, U.K.), and 10% human pooled serum (A+) supplied by the Belgian Red Cross (Croix-Rouge de Belgique, Namur, Belgium). The culture was observed and monitored through Giemsa-stained blood smears and standard light microscopy.

In vitro phenotypic analysis of *P. falciparum* erythrocytic stages (morphology and parasitaemia)

8TTE was isolated as described elsewhere and kept in a DMSO stock solution at − 20 °C [4]. Sorbitol synchronized parasites *P. falciparum* CQ-sensitive strain 3D7 were cultured in multiple plates (200 µL final well volume at 0.5% parasitaemia and 1% haematocrit). Each plate had six conditions: negative control (DMSO (0.1% v/v), 8TTE, ART, CQ, AVQ, or bestatin at 10 × or 100 × IC_{50}. For test A (Supplementary Fig. 1 A), parasites were exposed at 2 h post invasion (hpi), 12 hpi and 24 hpi, respectively, and incubated for 24 h. For test B (Supplementary Fig. 1B), parasites were cultured in the same six conditions exclusively at 100 × IC_{50} and incubated for 1 h, 24 h, 48 h, and 72 hpi. Each condition was performed in technical duplicate in three independent tests (n = 3). After incubation, each well was observed by Giemsa staining and light microscopy. The effects of the drug on the in vitro culture were determined by counting a total of 1000 RBCs per blood smear and taking note of parasitaemia and the developmental stage/condition parasites were in as per Supplementary Fig. 2.

Expression and purification of recombinant PfA-M17 and PfA-M1

A synthetic gene (Genecust, Luxembourg) encoding a cleavage site for the tobacco etch virus (TEV) protease fused to residues 84–605 of native *P. falciparum* leucyl aminopeptidase PfA-M17 (PlasmoDB PF3D7_1446200), was cloned into BamHI and SalI sites of the pET45b vector (Novagen), which appended a N-terminal hexahistidine tag. A similar strategy was used to clone the region encoding residues 192–1085 of the native *P. falciparum* alanyl aminopeptidase PfA-M1 (PlasmoDB PF3D7_1311800) into the KnpI and SalI sites of the pET45b vector, as previously described [14, 15].

After validation by Sanger sequencing (Beckman Coulter Genomics), the plasmids were transformed

into *Escherichia coli* Rosetta2 (DE3) (Novagen). Bacterial cultures were grown in auto-induced LB medium (Merck) supplemented with appropriate antibiotics (carbenicillin 50 µg/mL, chloramphenicol 34 µg/mL) during 24 h at 25 °C prior to bacterial extract preparations with BugBusterTM (Novagen). The clarified lysates were loaded onto Ni_2-charged HisTrap column (GE Healthcare), equilibrated in phosphate buffer supplemented with 20 mM imidazole, washed in the same buffer, and bound recombinant proteins were eluted in 200 mM imidazole for rPfA-M17 or 80 mM imidazole for rPfA-M1, in phosphate buffer. Eluted fractions were then purified by size exclusion chromatography on a Superdex 200 10 300 (equilibrated with HEPES 50 mM, NaCl 300 mM, $ZnCl_2$ 10 µM, 5% glycerol, pH 8.5 for rPfA-M17 and with Tris HCl 50 mM, NaCl 200 mM, $ZnCl_2$ 10 µM, pH 7.4 for rPfA-M1) using an Äkta purifier chromatography system.

Enzyme assays and kinetic analysis

Enzyme activities of rPfA-M17 and rPfA-M1, at 60 and 10 nM, respectively, were determined by measuring continuously the release of para-nitroaniline at 405 nm with leucine para-nitroanilide as substrate for rPfA-M17 (Km = 0.5 mM) and alanine para-nitroanilide for rPfA-M1 (Km = 1.5 mM) [16]. Assays were carried out on a HP/Agilent UV–Visible diode array spectrophotometer 8453, at 30 °C, in Tris HCl 50 mM, pH 8 for rPfA-M17, and pH 7.4 for rPfA-M1, with a final DMSO concentration of 1%. Initial velocities were measured with increasing concentrations of inhibitors and K_i values were determined by Dixon plots [17].

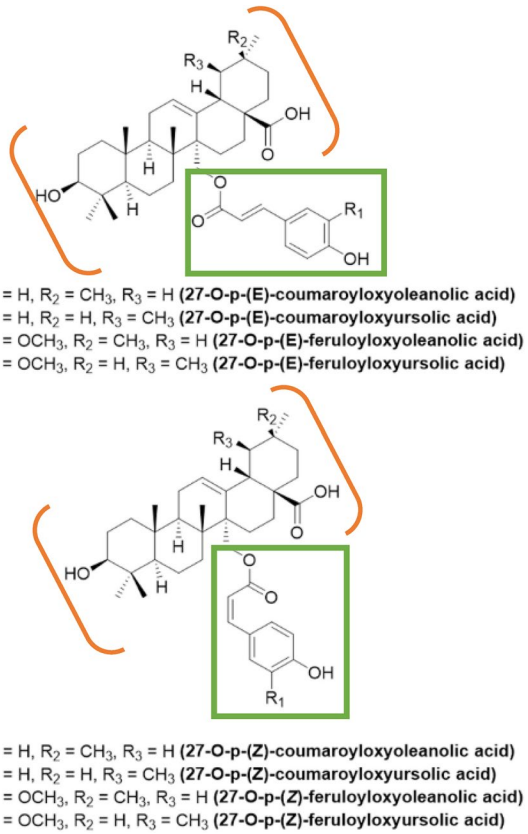

Fig. 1 Molecular structures of 8TTE isolated from *Keetia leucantha* (from Beaufay et al. [4]). In orange, terpenoid moiety and in green, the phenolic moiety

Table 1 Activity of *K. leucantha* extracts and isolated compounds found in the literature

Part Studied	Extract	Antiplasmodial activity (µg/ml)		Cytotoxicity (µg/ml)		Selectivity index	References
		3D7	W2	J774	WI38	WI38/3D7	
Leaf	Dichloromethane	13.8 ± 8.3	26.5 ± 9.5	91.5 ± 3.1	65.6 ± 1.3	4.8	[5]
	Methanol Water	> 100 > 100	ND ND	> 100 > 100	> 100 > 100	1.0 1.0	[5]
Twig	Dichloromethane	11.3 ± 3.8	15.8 ± 2.3	50.5 ± 4.2	> 100	8.8	[5]
	Methanol Water	> 100 > 100	ND ND	> 100 > 100	> 100 > 100	1.0 1.0	[5]
8TTE (1–8)		1.66 ± 0.54	0.88*	–	34.45 ± 1.10	20.75	[6]
1–2, 5–6		2.35 ± 0.44	–	–	ND	–	[6]
3–4, 7–8		2.93 ± 1.23	–	–	ND	–	[6]
Ursolic acid		31.5 ± 5	–	–	51 ± 0.10	0.2	[7]
Oleanolic acid		30.7 ± 4.6	–	–	28.9 ± 0.3	0.9	[7]

3D7 and W2 – *P. falciparum* strains, sensitive or resistant to CQ, respectively

J774 – macrophage-like cell line from BALB/c murine reticulum cell sarcoma

WI38 – human normal fibroblast cell line

ND – Not determined

* Tested once

Molecular docking

Molecular docking was carried out with the program AutoDock Vina 1.2.5 [18] (Vina) with the AD4Zn [19] parameter set. Receptor flexibility was mimicked by docking each ligand to 12 different PfA-M17 conformations corresponding to the 12 chains of the PDB entry 3t8w [10]. Missing atoms in the PDB receptor file were neglected as they are distant from the activate site. All non-protein molecules were removed prior to addition of atomic charges & polar hydrogens with AutoDockTools 1.5.7 [20] (ADT). In the resulting PDBQT receptor files the charge of the Zn(II) ions were set to zero (in agreement with the AD4Zn parametrization) and renamed to Zn. Finally, the PDBQT receptor files were analyzed for the eventual placement of auxiliary TZ atoms with the python script zinc_pseudo.py (github.com/ccsb-scripps/AutoDock-Vina/tree/develop/example/autodock_scripts); the script detected & added a single TZ atom for each receptor conformation. Ligands were loaded as neutral (protonated) species into ADT to merge non-polar hydrogens and to add atomic charges. For the (*E*)-isomers **1**–**4** the furelic-like moiety was docked in a fully planar conformation by choosing the double bond and attached single bonds as non-rotatable. Two and four configurations were considered for **1** & **2** and **3** & **4**, respectively, corresponding to the different orientations of the carbonyl double bond and the methoxy group relative the double bond. For the (*Z*)-isomers **5**–**8** only the double bond of the ferulic-like moiety was chosen as non-rotatable. The resulting PDBQT-ligand files were then modified to convert the ligands into their deprotonated forms. The acidic proton (last entry of the file) was removed, and the charges of the carboxylic oxygens was set to −0.647*e* (which corresponds to the charge of the carboxylic oxygen of ASP and GLU residues, respectively). The charge of the carboxylic carbon of the ligand was adjusted to obtain an overall charge of −1. Affinity grid maps were calculated with AutoGrid 4.2.7; the required GPF files were created with the script prepare_gpf4zn.py (github.com/ccsb-scripps/AutoDock-Vina/tree/develop/example/autodock_scripts) using the coordinates of the auxiliary TZ atom as the center of the grid. Docking with Vina was performed with an exhaustiveness of 128 and "ad4" scoring. The reported score corresponds to the "Estimated Free Energy of Binding" as given in the Vina output. For each ligand-receptor combination the score and pose of the top-ranked binding mode was extracted. For a given ligand, three scoring criteria were determined: 1) best overall score when comparing the scores for the twelve receptor conformations; 2) mean values of those 12 scores; and 3) the corresponding standard deviation.

HPLC–MS metabolomics characterization of *P. falciparum* trophozoites

Metabolomics assays were performed as described by Allman et al. [13]. Briefly, the *P. falciparum* cultures were microscopically verified for presence of sufficient trophozoite stage synchronicity at the desired parasitaemia before they were magnetically purified. The sample of ~ 95–100% pure infected erythrocytes was distributed into 6-well plates at ~ 0.2% haematocrit and incubated for a 1-h recovery period. After recovery, the parasites were exposed to 8TTE (see Table 1 for reference [6]) or reference compounds at $10\times IC_{50}$ for 2.5 h. ART (Sigma-Aldrich 361593, AVQ (Sigma-Aldrich A7986), and CQ (Sigma-Aldrich C6628) were used as metabolomics profile controls. After pelleting and washing in ice cold PBS pH 7.4, infected red blood cells were resuspended in 1 ml of 90% methanol with 0.5 µM [$^{13}C_4$,$^{15}N_1$] aspartate as an internal control. Supernatants were dried under nitrogen flow and stored at − 80 °C before being resuspended to 10^6 former cells/µL in HPLC-grade water with 1 µM chlorpropamide as an additional internal control for reverse phase UHPLC-MS analysis on a Thermo Exactive Plus orbitrap. 10 µL were injected on a C18 column (Waters XSelect HSS T3 2.5 µM, catalog no. 186006151) and ran using a 25-min gradient of 3% aqueous methanol–15 mM acetic acid–10 mM tributylamine-2.5 µM medronic acid ion pairing agent (A) and 100% methanol (B). Detection was performed in negative-ion mode, using a scan range of 85 to 1,000 m/z and a resolution of 140,000 at m/z 200.

After data acquisition,.raw files were converted to centroided.mzML files using MSConvert of the ProteoWizard package [21] and then visualized, processed and annotated with El-MAVEN [22]. The internal standard intensity was used to evaluate technical reproducibility, and peaks were manually identified based on the proximity of the retention time with the targeted library, *m/z* and the signal/blank ratio. Chlorpropamide was used to correct the peak areas per metabolite for instrument variation during the run. Subsequently, blank signals were subtracted, and metabolites were filtered based on the relative standard deviation (RSD, Standard Deviation/Mean) of the pooled quality control samples and removed when they showed low repeatability across technical replicates (RSD > 25%). The remaining metabolites were analyzed in two ways: log2 fold changes were displayed in a self-organizing map, or metaprint [13], for profile comparison; or loaded directly in MetaboAnalyst 5.0 for statistical analysis [23].

Results

Parasitic morphology and phenotype after 8TTE treatment

Direct microscopy-based visualization of *Plasmodium* spp. morphology is a relatively straightforward method to relate the in vitro activity of a compound with a potential biological effect [10]. Multiple antimalarial drugs induce characteristic effects that can be visualized by routine staining and light microscopy, such as chromatin condensation for ART derivatives [24, 25], digestive vacuole (DV) swelling or its absence for a few haemoglobin catabolism inhibitors [10, 26], or developmental arrest [25, 27, 28]. To gain insight into the mode of action of 8TTE, morphologic phenotypic analysis was performed using two separate tests: stage-specific (test A) and 72 h exposure (test B) (Supplementary Fig. 1A, Fig. 2A and G). For test A, parasites were synchronized by sorbitol and then treated for 24 h, beginning at three different developmental stages: early-ring (2–6 hpi), trophozoite (12–16 hpi), and schizont (24–28 hpi). Treatments included 8TTE, and standards of ART, CQ, AVQ, and bestatin at 10 and $100 \times IC_{50}$. Representative Giemsa-stained smears can be found in Fig. 2B. ART treatment resulted in parasite death at the ring, trophozoite, and schizont stages, as marked by the presence of pyknotic bodies [24, 25]. CQ exhibited a similar effect at the trophozoite and schizont stages, and a static morphology at ring stage [10, 26, 29]. AVQ treatment blocked the ring to trophozoite transition as expected [29]. Finally, parasite incubation with bestatin, which is known to inhibit both PfA-M1 and PfA-M17, presented with a DV swelling phenotype, as previously reported [10, 30]. This DV swelling is attributed specifically to PfA-M1 inhibition, since other PfA-M17-specific inhibitors do not result in this phenotype [10, 30]. DV swelling is associated with disruptions to haemoglobin degradation pathways that result in an accumulation of haemoglobin-derived peptides in the DV [30–33]. 8TTE resulted in changes to the cytoplasm that were perceptible during the trophozoite incubation, revealing irregular parasitic forms. Ring-stages were visible in the schizont-treated group, which was similar to the no drug control at the turn of the lifecycle, although the 8TTE-treated samples had morphological changes. This is further corroborated by the percentage of viable parasites in this group of 40.1% ± 17.9 (Fig. 2E) in comparison to 92.2% ± 7.1 in the positive control. Quantification of the viability of all drug-treated parasites based on morphology (Fig. 2C, D and E) revealed a higher percentage of viable parasites when they were incubated with 8TTE at a later stage (24–28 hpi) than with other treatments (Fig. 2E). The percentage of ring-stages in this group was higher compared to other antimalarial drugs (Fig. 2F). This suggests a stage-specific effect during ring and trophozoite stages, particularly because the rings produced following schizont incubation display absence of nucleus and irregular membranes (Fig. 2B, microscopical observation). After 8TTE treatment at 24–28 hpi, a notable proportion of remaining trophozoites was observed, suggesting a possible stage-dependent effect, although a general delay in the intraerythrocytic cycle cannot be ruled out (Fig. 2F).

Next, parasites were exposed for 72 h in test B (Fig. 2G), to observe morphological and ultrastructural changes at four timepoints after treatment: 1 h, 24 h, 48 h and 72 h (Fig. 2H). The earliest effect detected at 1 h can be attributed to ART, a known fast-acting drug that affects early ring-stages [11]. At the same timepoint, CQ treated ring-stages already show irregular parasite membranes. At 24 h post-treatment, all treated parasites have morphological changes relative to the control with developmental arrest concurrent with smaller sizes and a lack of visible haemozoin. At 48 h post-treatment, 8TTE-treated parasites appear morphologically large and disorganized and do not resemble parasites treated with the other antimalarials. By 72 h, the 8TTE-treated parasites appear to have developmentally arrested, perhaps entering a similar pyknotic state as seen with ART and CQ treatments (Fig. 2H).

Evaluation of PfA-M17 and PfA-M1 inhibition by 8TTE and its moieties

To investigate the potential targets of 8TTE, enzymatic tests were performed using recombinant versions of two known aminopeptidases, PfA-M1 and PfA-M17. These enzymes were chosen because betulinic acid, a triterpenic acid close to the triterpenic backbones of 8TTE, was shown to inhibit mammalian aminopeptidase N [34] so an activity on aminopeptidases was suspected. In *P. falciparum* parasites, these proteins are both localized to the cytosol [30, 35], where they catalyze the final steps of haemoglobin catabolism [30, 35, 36] and can be inhibited by bestatin [30, 35, 36]. These metalloaminopeptidase enzymes were also selected due to their recognized crucial role in the final hydrolysis and cleavage of short haemoglobin-derived peptides that occur in the cytosol [29, 31, 37–40]. The released amino acids are essential for protein biosynthesis, redox homeostasis, and to maintain osmotic pressure [31, 39]. As the morphologic assessment showed no effects of 8TTE on the DV, these cytosolic enzymes were selected. The triterpene ursolic acid and phenolic ferulic acid (parts of the 8TTE esters) were also tested to evaluate whether the enzymatic activity could pertain solely to the triterpenic or phenolic moieties of 8TTE.

Enzyme activities of rPfA-M17 and rPfA-M1 were determined by continuously measuring the release of para-nitroaniline at 405 nm with leucine para-nitroanilide

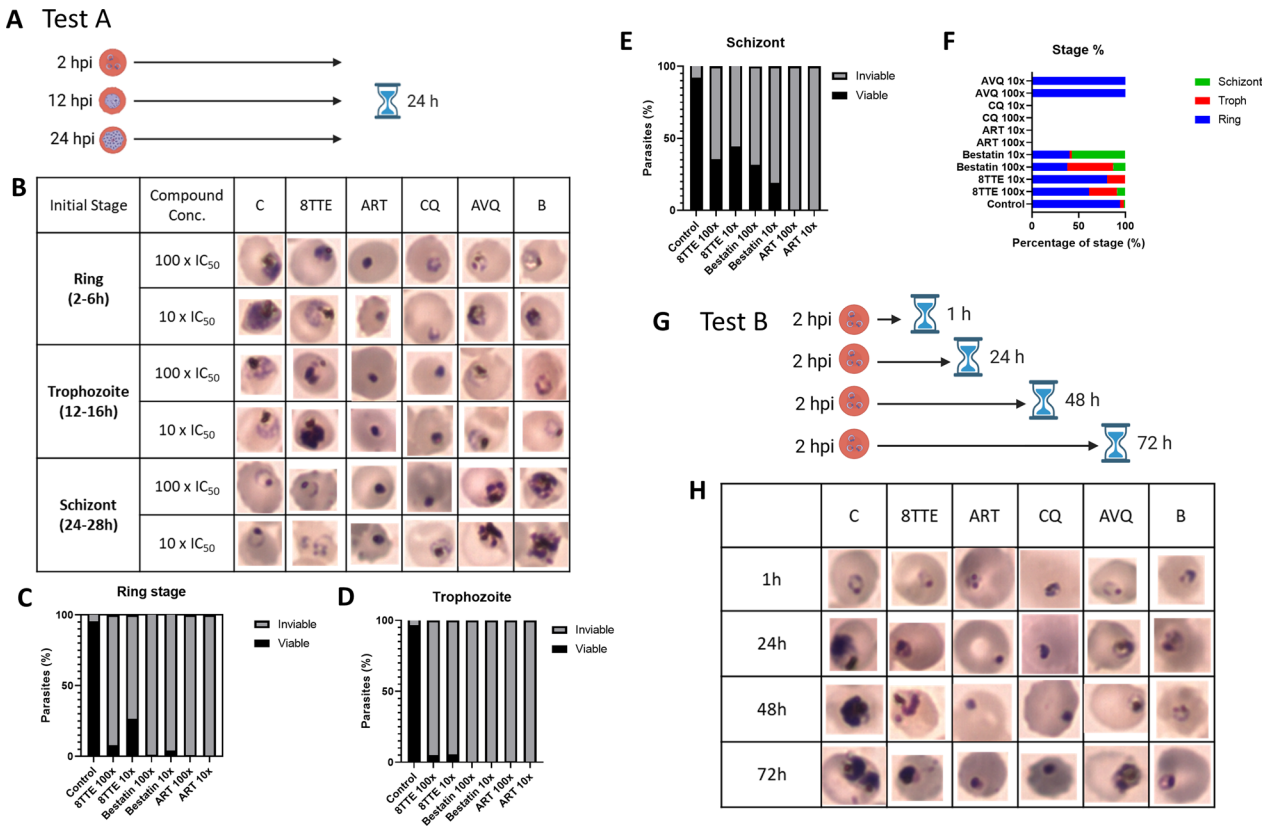

Fig. 2 **A** Test design of in vitro phenotypic analysis of *P. falciparum* erythrocytic stages – Test A. hpi – hours post invasion. **B** Representative morphologies of parasites in Test A after incubation for 24 h at each specific stage under 8TTE, ART (ART), CQ (CQ), AVQ (AVQ), bestatin (**B**), and no treatment (**C**) at 100 and tenfold their respective IC_{50}. The percentage of drug-affected parasites for groups with no treatment (control), 8TTE and bestatin treatments with 100 and tenfold their respective IC_{50}, including morphological viability to continue the lifecycle, for each stage: ring (**C**), trophozoite (**D**), and schizont (**E**). **F** Stage abundances of viable parasites observed after incubation for 24 h at 24–28 h pi (schizont) for control, bestatin and 8TTE groups. **G** Test design of in vitro phenotypic analysis of *P. falciparum* erythrocytic stages – Test B. **H** Representative morphologies of parasites after incubation for 1 h, 24 h, 48 h and 72 h under 8TTE, ART, CQ, AVQ, B, at 100-fold their respective IC_{50}, and the control group. (All percentage levels are the average of triplicate tests and double replicates.)

as substrate for rPfA-M17 (Km = 0.5 mM) and alanine para-nitroanilide for rPfA-M1 (Km = 1.5 mM) [16]. Initial velocities were measured with increasing concentrations of inhibitors and K_i values were determined by Dixon plots [17]. 8TTE was found to be active against rPfA-M17 with an inhibition constant (K_i) in the single digit micromolar range (1.1 µM), with no effect on rPfA-M1 below 20 µM (Table 2). Interestingly, ursolic acid and ferulic acid did not show specific activity for either enzyme, indicating that both the triterpenic skeleton and the phenolic group must be linked, as in 8TTE, to have a specific interaction with PfA-M17. The K_i of 8TTE for rPFA-M17 is indicative of a differential selectivity, and, as such, in silico molecular docking strategies were applied to confirm the interface leading to this affinity.

Molecular docking studies of 8TTE and their moieties with rPfA-M17

Molecular docking revealed two main, possible binding modes for the 8TTE compounds with the enzyme rPfA-M17. In the top-ranked and most common binding mode, the phenol (or catechol) group is complexed to the Zn(II) ions and the carboxylic acid typically interacts with the side-chain of Lys386 (Fig. 3A). In the less favorable and less common binding mode, the carboxylic group is complexed to the Zn(II) ions and the ester carbonyl usually interacts with Lys386 (Fig. 3B). All 8TTE components have the same level of affinity (score < −10). To further investigate the active moiety responsible for the binding activity, the simulation was repeated on the unesterified triterpenic part (Table 3), with an additional test for ferulic acid. As expected from the enzymatic tests, these compounds score significantly worse compared to the 8TTE compounds (higher scores).

8TTE-treated parasite metabolomics profile

To further explore the mode of action of 8TTE, high performance liquid chromatography-high resolution mass spectrometry (HPLC-HRMS) was used to perform a metabolomic analysis after incubating the compound (at $10\times IC_{50}$) with synchronized and purified parasite cultures (>95% late trophozoite stages) for 2.5 h. The metabolic response to 8TTE was compared to parasites treated with ART, AVQ and CQ (Fig. 4). The self-organizing MetaPrints (Fig. 4A) reveal that 8TTE effects resemble the malaria parasite response to ART, with the greatest effect of the treatment being a negative log2 fold change for haemoglobin-derived peptides. Therefore, the metabolomic analysis suggests that parasite exposure to 8TTE results in disruption of normal haemoglobin digestion, perhaps by PfA-M17 [13].

An ANOVA test was also performed, which identified 18 metabolites showing a significant (p-value < 0.05) variation compared to the mean normalized intensity across groups (Fig. 4B). The heatmap of the 18 metabolites can be separated into two parts: the bottom part with a relative decrease in abundance for most haemoglobin-derived peptides for samples treated with ART and 8TTE, and the top part where the fold change varies between treatments and metabolites. The 8TTE heatmap identifies several metabolites with a different fold change from all other groups, *e.g.,* pyroglutamic acid and hexose. The clustering of ART and 8TTE (Fig. 4B) further suggests a similar mode of action including the disruption of haemoglobin digestion.

Table 2 Kinetic evaluation of inhibition (K_i) of 8TTE and ursolic acid on cytosolic aminopeptidases

	rPfA-M1	rPfA-M17
8TTE	> 20 µM	1.1 ± 0.2 µM
Ursolic acid	> 20 µM	> 20 µM
Ferulic acid	> 20 µM	> 20 µM

Discussion

Traditional medicine is used globally by over 80% of the human population as a complement to modern medicine [41]. Natural compounds are an important source of innovative scaffolds that inspire new drug leads, especially so for antimalarial agents [41, 42]. The history of *K. leucantha* in this context has led to the discovery of 8TTE, a mixture of triterpenic esters with antiplasmodial activity, effective in vitro against both CQ sensitive and resistant strains of *P. falciparum* [4, 6, 8]. Considering the need for innovative antimalarial treatments due to rising drug resistance [1], this study sought to describe the mode of action of 8TTE.

Phenotypic studies demonstrated 8TTE-based alterations to asexual blood stage parasite development as compared to four antimalarial compounds with different modes of action – ART, CQ, AVQ, and bestatin – whose effects are dependent on the developmental

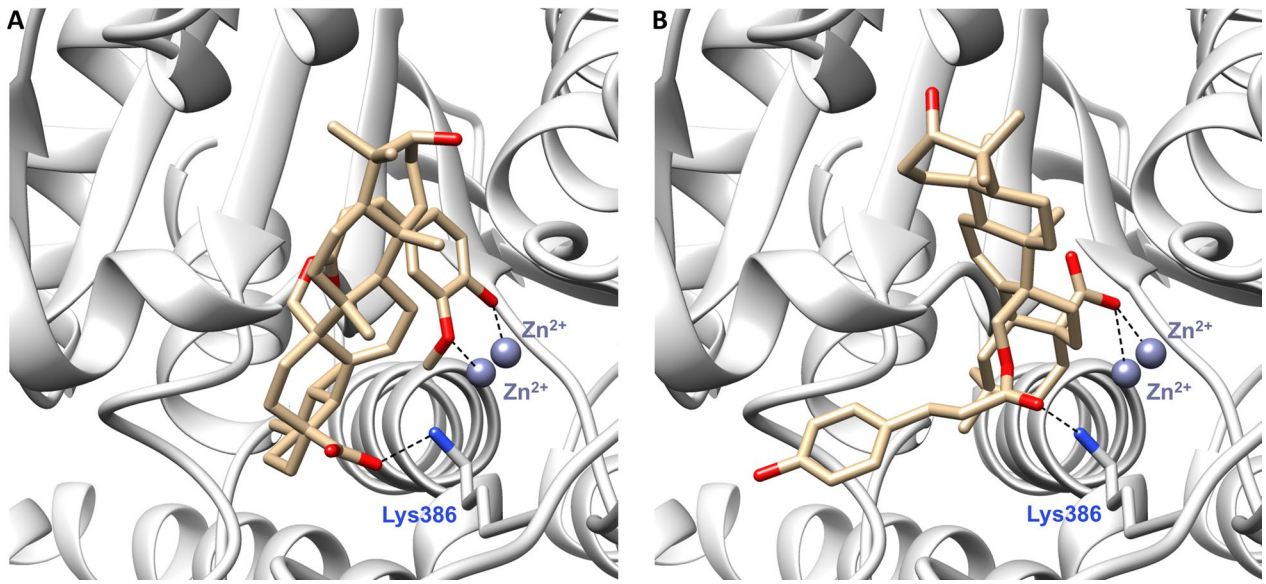

Fig. 3 Binding modes of 8TTE compounds when docked to PFAM17. **A** Top-ranked catechol-complexed pose of 8. **B** Alternative carboxylate-complexed mode for compound 1. Protein (white) is shown as cartoon model, the ligands (tan) & Lys386 as think sticks and the metal centers as small spheres. Hydrogen atoms are removed for clarity. Dashed lines indicate ligand–metal complexations or polar ligand–protein interactions.

Table 3 AD4Zn docking scores; all values in kcal/mol

Compound	Top	Mean	SD
Ferulic acid	− 7.3	− 7.0	0.2
Ursolic acid[$]	− 8.8	− 8.3	0.5
(3β)−3,27-dihydroxyurs-12-en-28-oic acid[$]	− 8.4	− 8.6	0.7
Oleanolic acid[$]	− 9.2	− 8.2	0.6
(3β)- 3,27-dihydroxyolean-12-en-28-oic acid[$]	− 9.0	− 8.4	0.5
8TTE—1[£]	− 11.2	− 10.4	0.6
8TTE—2[£]	− 11.4	− 10.8	0.5
8TTE—3[£]	− 13.0	− 12.1	0.7
8TTE—4[£]	− 13.2	− 12.7	0.3
8TTE—5	− 11.9	− 10.9	0.6
8TTE—6	− 12.0	− 11.4	0.5
8TTE—7	− 13.0	− 12.2	0.7
8TTE—8	− 13.5	− 12.6	0.7

[$] Structures can be found in Supplementary Fig. 3

[£] Different ligand configurations were docked (see Methods); the overall best-scoring ligand configuration is reported ("Top") as well as the mean and standard deviation when averaging over the best-scoring ligand configurations for each of the twelve receptor conformations ("Mean" & "SD")

For each ligand the overall top-ranked score (Top) as well as the mean value (Mean) when averaging over the best score of the twelve receptors and the corresponding standard deviation (SD)

stages [10, 11, 29, 30]. Parasites treated with 8TTE displayed clear morphological changes during ring and trophozoite incubations, with a higher degree of survival after schizont incubation compared to other treatments. This is consistent with an activity onset early in asexual blood stage development. The morphologic effects, however, were markedly different to the other antimalarial drugs tested. Cytosolic changes seen in parasites after 24 h exposure to 8TTE, with non-circular shapes containing an accumulation of dense material which could be due to haemoglobin accumulation (Fig. 2B, 8TTE treatment trophozoite group at $10\times IC_{50}$) [32]. A dark, swollen DV has previously been associated with the inhibition of endopeptidases, such as falcipains [43, 44] while inhibitors of aminopeptidases such as PfA-M1, induce a translucent, enlarged DV due to the accumulation of short oligopeptides [10, 32]. At 72 h, ART, CQ and 8TTE all result in the formation of pyknotic bodies, although of different sizes. E64, a falcipain inhibitor, also leads to dark swollen DV but the parasites remain alive until at least 60 h post treatment. This was not observed with 8TTE [10, 30]. Therefore, treatment with 8TTE likely exerts a different mode of action on the parasites with an early onset that could potentially affect haemoglobin metabolism outside the parasite DV [11].

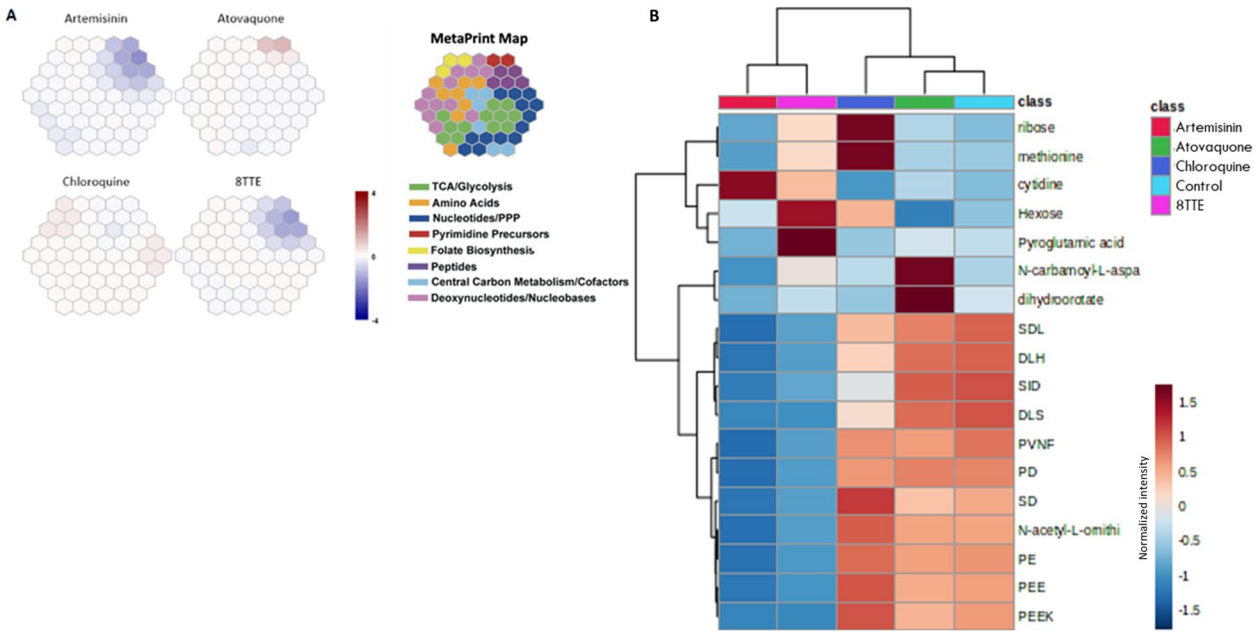

Fig. 4 (**A**) Metabolic effects of the study group compounds on malaria parasites showing the Metaprint representation of the data (adapted from Allman et al. 2016). [13] (**B**) Heatmap based on the mean normalized intensity of UHPLC-MS data with a clustering dendrogram (distance measure: Euclidean, clustering algorithm: Ward) of the metabolites scored as significant by ANOVA (p-value < 0.05). *DLH* aspartyl-leucyl-histidine, *DLS* aspartyl-leucyl-serine, *PE* Prolyl-Glutamate, *PD* Prolyl-Aspartate, *PEE* prolyl-glutamyl-glutamate, *PEEK* Prolyl-Glutamyl-Glutamyl-Lysine, *PVNF* L-prolyl-L-valyl-L-asparaginyl-L-phenylalanine, *SD* serylaspartic acid, *SID* Seryl-isoleucyl-asparate, *SDL* seryl-aspartyl-leucine

8TTE displays a selective inhibition for PfA-M17, a bimetallic zinc aminopeptidase with a narrow substrate specificity for leucine and tryptophan that removes these amino acids from N-terminus of peptides, compared to the wide substrate specificity of the mono-metallic zinc aminopeptidase PfA-M1 [30, 37, 39, 40, 45, 46]. Genetic assays with PfA-M17 revealed its deletion is non-viable, suggesting that it is necessary for parasite survival [30, 31, 39, 45]. The specificity of PfA-M17 for leucine, the most abundant amino acid in human haemoglobin, has been linked with the necessity to obtain isoleucine from the host through exchange via specific channels, although it is possible that this enzyme has other essential roles [10, 30, 45]. A-M17 are widely conserved across Apicomplexan parasites, including *Babesia* spp., *Eimeria tenella*, and *Toxoplasma gondii,* further attesting their potential as antiparasitic targets [38, 39].

PfA-M17 inhibition has previously been reported to halt the development of rings into trophozoite stage parasites [10]. A recent study by Edgar et al. also found that multiple digestive vacuoles are found in *P. falciparum* parasite strains in which PfA-M17 is knocked down [10, 30]. In the present study, a lack of development into trophozoites upon treatment with 8TTE during a 72 h drug exposure was also found (Fig. 2H). No perceivable changes to the DV were observed in 8TTE treated parasites, which confirmed the lack of PfA-M1 inhibition. Additionally, 8TTE is shown to affect ring-stage parasites which is not the case when selective PfA-M1 (PlasmoDB PF3D7_1311800) inhibitors are tested at this stage [14, 46]. Rather, PfA-M1 inhibitors show an effect on the reinvasion process, leading to fewer free merozoites and impaired reinvasion, which is also not seen after 8TTE treatment [46]. The ring-stage percentage after incubation with 8TTE during the schizont stage is higher than any other treatment group (Fig. 2E), which would indicate that 8TTE does not affect merozoite release or RBC invasion.

Docking studies using PfA-M17 suggest that the 8TTE compounds bind either with their phenol/catechol or the carboxylic group to the enzyme's metal center. While inhibition of metalloenzymes by catechol fragments has been reported for Fe(II/III)-Metallo-Protein (MP), it is unclear if this interaction is direct (or water-mediated) and if at all feasible for dinuclear Zn(II)-MPs such as PfA-M17 [47]. The lack of enzymatic activity of ursolic acid and ferulic acid, coupled with the lower docking scores when individual groups are lost (such as the ferulic moiety or the triterpenic carboxy group), indicates that the entire triterpenic phenolic ester structure is critical.

Metabolomic analysis revealed related metabolic effects on *P. falciparum* between ART and 8TTE that are distinct from CQ treatment effects. CQ and ART are known to have different targets and modes of action, despite both affecting haemoglobin metabolism: CQ acts on heme biomineralization, while ART has pleiotropic effects including haemoglobin uptake [11]. ANOVA analysis of the significantly altered metabolites across treatments confirms a lower abundance of haemoglobin-derived peptides in parasites treated with 8TTE and ART, which is also distinct from CQ treatment. If PfA-M17 inhibition was the main effect of 8TTE, a decrease of free leucine was also to be expected, considering that the relevant peptides (with N-terminal leucine) would no longer be cleaved. Unfortunately, leucine was not reliably detected, so no definitive conclusions can be made. However, due to the similarity shown thus far with the profile of parasites treated with ART, it is plausible that 8TTE affects the DV or early haemoglobin metabolism through mechanisms that don't visibly swell the DV, *i.e.,* targets enzymes other than PfA-M1 and falcipains [43].

8TTE is a unique triterpene derivative with high antiplasmodial activity and selectivity [5–7]. A study by Freire et al. demonstrated that the antiplasmodial activity of *K. leucantha* twigs is directly linked to the presence of 8TTE [6, 9]. Other triterpenic acid analogues have been synthesized and investigated for their potential mode of action against *Plasmodium* [6], revealing a weak capacity to inhibit β-haematin formation and an inability to inhibit mitochondrial membrane potential, which aligns with the metabolomic results of the present study [48]. Notably, triterpenes can also disturb membranes due to their lipophilic nature, though this interaction may be not specific [8].

Interestingly, only a few triterpenic esters are known for their antiplasmodial activity aside from the ones reported in *K. leucantha* [6]. Messagenic acids A and B were isolated from *Gardenia saxatilis* (Rubiaceae) and displayed IC_{50} of 1.5 and 3.8 µg/ml, respectively, on a multidrug resistant strain of *P. falciparum* (K1) [49]. A mixture of uncarinic acid E and 27-*O*-*p*-(*E*)-coumaroyloxyursolic acid isolated from the same plant also showed antiplasmodial activity on K1 (2.9 µg/ml) [49]. Triterpenic esters from the root bark of *Ziziphus cambodiana* (Rhamnaceae) also elicited a few compounds with interesting IC_{50} (0.9 and 3.7 µg/ml) on the same parasite strain [50]. These IC_{50} are close to those reported in Table 1 for 8TTE, despite the strains being different. More importantly, activity was correlated to the coumaric moieties and the esterification on the 27-position [6]. Recently, 27-*O*-coumaroyl derivatives have been shown to have more antiplasmodial activity (strain 3D7) than 3-*O*-coumaroyl derivatives, but the presence of an ester in C-3 doesn't seem to be the only ruling factor in this decline of activity against *Plasmodium* [7]. Indeed, the docking study with 8TTE and PfA-M17 shows that the 27 C

substitution is important for this enzymatic interaction It remains to be determined if it is the position of the esterification, or the loss of the phenolic moiety that influences the antiplasmodial activity.

The presented results show that 8TTE could target multiple aspects of haemoglobin metabolism including PfA-M17. Studies to confirm this hypothesis and develop this scaffold to have improved bioavailability could prove invaluable to revitalizing antimalarial drug discovery.

Conclusion

This study finds that 8TTE elicits a morphologic phenotype against *P. falciparum* that is consistent with an early-ring stage activity onset with possible activity related to haemoglobin metabolism. Enzymology assays revealed a specific inhibition of PfA-M17, an essential metalloaminopeptidase, but not of PfA-M1. Molecular docking confirmed a high binding score for all 8TTE mixture constituents to PfA-M17 and revealed the importance of both the catechol/phenol and triterpenic moieties for 8TTE activity on PfA-M17. Metabolomic profiling shows confluence between the parasite response to ART and 8TTE treatments, with haemoglobin-derived peptide abundances reduced, and downstream effects suggesting a perturbation of the amino acids pool. Further structure–activity and medicinal chemistry studies are warranted to elaborate on these findings and the potential for 8TTE-related molecules to serve as future antimalarial drugs.

Abbreviations

8TTE	Eight triterpenic esters
ART	Artemisinin
AVQ	Atovaquone
CQ	Chloroquine
DV	Digestive vacuole
HPLC-HRMS	High performance liquid chromatography–high resolution mass spectrometry
MP	Metallo-protein
RSD	Relative standard deviation

Supplementary Information

The online version contains supplementary material available at https://doi.org/10.1186/s12936-025-05762-3.

Supplementary file 1

Acknowledgements

The authors would like to acknowledge the Huck Institutes' Metabolomics Core Facility (RRID:SCR_023864) for maintenance of the Thermo Exactive Plus.

Author contributions

LM drafted the manuscript and carried out most of the experiments. GWR contributed to the metabolomics section. MSchmitt carried out the expression of recombinant proteins and the enzymatic assays. SA and MSpichty performed molecular docking assays. JB and CB extracted and identified the molecules in the study. IF, ML, MF and JQL supervised, reviewed and oversaw the research platforms, projects and multiple revisions of this manuscript. All authors read and approved the final manuscript.

Funding

This work was supported by the Belgian National Fund for Scientific Research (FNRS, grant PDR T.0092.20) and by the Fondation Léon Fredericq. GR was supported by a Penn State Eberly Research Fellowship and grant R21AI174085 from the NIH. Funding to M.L. was supported by the Eberly College of Science and the Huck Institutes of the Life Sciences at The Pennsylvania State University and NIH grant R21AI174085. Support for CB, JB, IF and MS by a Tournesol/Hubert Curien program and in parts by ANR-12-BS07-0020 is also acknowledged.

Data availability

This data is available at the NIH Common Fund's National Metabolomics Data Repository (NMDR) website, the Metabolomics Workbench, https://www.metabolomicsworkbench.org where it has been assigned Study ID: ST004425.

Declarations

Ethics approval and consent to participate

Not applicable.

Consent for publication

Not applicable.

Competing interests

The authors declare no competing interests.

Received: 22 September 2025 Accepted: 18 December 2025
Published online: 02 January 2026

References

1. WHO. World malaria report 2024: addressing inequity in the global malaria response. Geneva, World Health Organization, 2024. https://www.who.int/teams/global-malaria-programme/reports/world-malaria-report-2024.
2. Tse EG, Korsik M, Todd MH. The past, present and future of anti-malarial medicines. Malar J. 2019;18:193.
3. Antonova-Koch Y, Meister S, Abraham M, Luth MR, Ottilie S, Lukens AK, et al. Open-source discovery of chemical leads for next-generation chemoprotective antimalarials. Science. 2018;362:eaat9446.
4. Beaufay C, Henry G, Streel C, Bony E, Hérent M-F, Bero J, et al. Optimization and validation of extraction and quantification methods of antimalarial triterpenic esters in *Keetia leucantha* plant and plasma. J Chromatogr B. 2019;1104:109–18.
5. Bero J, Ganfon H, Jonville MC, Frédérich M, Gbaguidi F, DeMol P, et al. In vitro antiplasmodial activity of plants used in Benin in traditional medicine to treat malaria. J Ethnopharmacol. 2009;122:439–44.
6. Bero J, Hérent MF, Schmeda-Hirschmann G, Frédérich M, Quetin-Leclercq J. In vivo antimalarial activity of *Keetia leucantha* twigs extracts and in vitro antiplasmodial effect of their constituents. J Ethnopharmacol. 2013;149:176–83.
7. Catteau L, Schioppa L, Beaufay C, Girardi C, Hérent M-FF, Frédérich M, et al. Antiprotozoal activities of triterpenic acids and ester derivatives isolated from the leaves of *Vitellaria paradoxa*. Planta Med. 2021;87:860–7.
8. Beaufay C, Hérent M-F, Quetin-Leclercq J, Bero J. In vivo anti-malarial activity and toxicity studies of triterpenic esters isolated form *Keetia leucantha* and crude extracts. Malar J. 2017;16:406.
9. Freire RT, Bero J, Beaufay C, Selegato DM, Coqueiro A, Choi YH, et al. Identification of antiplasmodial triterpenes from *Keetia* species using NMR-based metabolic profiling. Metabolomics. 2019;15:27.
10. Harbut MB, Velmourougane G, Dalal S, Reiss G, Whisstock JC, Onder O, et al. Bestatin-based chemical biology strategy reveals distinct roles for malaria M1- and M17-family aminopeptidases. Proc Natl Acad Sci U S A. 2011;108:E526–34.
11. Mamede L, Ledoux A, Tullio PD, Quetin-Leclercq J. Recent metabolomic developments for antimalarial drug discovery. Parasitol Res. 2022;121:3351–80.

12. Ledoux A, Cao M, Jansen O, Mamede L, Campos PE, Payet B, et al. Antiplasmodial, anti-chikungunya virus and antioxidant activities of 64 endemic plants from the Mascarene Islands. Int J Antimicrob Agents. 2018;52:622–8.
13. Allman EL, Painter HJ, Samra J, Carrasquilla M, Llinás M. Metabolomic profiling of the malaria box reveals antimalarial target pathways. Antimicrob Agents Chemother. 2016;60:6635–49.
14. Bounaadja L, Schmitt M, Albrecht S, Mouray E, Tarnus C, Florent I. Selective inhibition of PfA-M1, over PfA-M17, by an amino-benzosuberone derivative blocks malaria parasites development in vitro and in vivo. Malar J. 2017;16:382.
15. Alonso IP, Bounaadja L, Sánchez L, Rivera L, Tarnus C, Schmitt M, et al. Aqueous extracts of marine invertebrates from Cuba coastline display neutral aminopeptidase inhibitory activities and effects on cancer cells and *Plasmodium falciparum* parasites. Indian J Nat Prod Resour. 2017;8:107–19.
16. Salomon E, Schmitt M, Mouray E, McEwen AG, Bounaadja L, Torchy M, et al. Aminobenzosuberone derivatives as PfA-M1 inhibitors: molecular recognition and antiplasmodial evaluation. Bioorg Chem. 2020;98:103750.
17. Segel IH. Enzyme Kinetics: behavior and analysis of rapid equilibrium and steady-state enzyme systems. Wiley Classics Library; 1993;992 p.
18. Eberhardt J, Santos-Martins D, Tillack AF, Forli S. AutoDock Vina 1.2.0: new docking methods, expanded force field, and python bindings. J Chem Inf Model. 2021;61:3891–8.
19. Santos-Martins D, Forli S, Ramos MJ, Olson AJ. AutoDock4 Zn : an improved autodock force field for small-molecule docking to zinc metalloproteins. J Chem Inf Model. 2014;54:2371–9.
20. Morris GM, Huey R, Lindstrom W, Sanner MF, Belew RK, Goodsell DS, et al. AutoDock4 and AutoDockTools4: automated docking with selective receptor flexibility. J Comput Chem. 2009;30:2785–91.
21. Kessner D, Chambers M, Burke R, Agus D, Mallick P. ProteoWizard: open source software for rapid proteomics tools development. Bioinformatics. 2008;24:2534–6.
22. Agrawal S, Kumar S, Sehgal R, George S, Gupta R, Poddar S, et al. El-MAVEN: a fast, robust, and user-friendly mass spectrometry data processing engine for metabolomics. In: Buchwald's Atlas of Metabolic and Bariatric Surgical Techniques and Procedures Elsevier; 2019. p. 301–21.
23. Pang Z, Chong J, Zhou G, de Lima Morais DA, Chang L, Barrette M, et al. MetaboAnalyst 5.0: narrowing the gap between raw spectra and functional insights. Nucleic Acids Res. 2021;49:W388–96.
24. Dogovski C, Xie SC, Burgio G, Bridgford J, Mok S, McCaw JM, et al. Targeting the cell stress response of *Plasmodium falciparum* to overcome artemisinin resistance. PLoS Biol. 2015;13:e1002132.
25. Asahi H, Inoue S-I, Niikura M, Kunigo K, Suzuki Y, Kobayashi F, et al. Profiling molecular factors associated with pyknosis and developmental arrest induced by an opioid receptor antagonist and dihydroartemisinin in *Plasmodium falciparum*. PLoS ONE. 2017;12:e018874.
26. Khan J, Kaushik M, Singh S. Molecular mechanisms of action and resistance of antimalarial drugs. Mandal S, Paul D (eds.); Bacterial Adaptation to Co-resistance. Springer, Singapore. 2019;267–96.
27. Jiménez-Díaz MB, Ebert D, Salinas Y, Pradhan A, Lehane AM, Myrand-Lapierre M-E, et al. (+)-SJ733, a clinical candidate for malaria that acts through ATP4 to induce rapid host-mediated clearance of *Plasmodium*. Proc Natl Acad Sci U S A. 2014;111:E5455–62.
28. Chen M, Theander TG, Christensen SB, Hviid L, Zhai L, Kharazmi A. Licochalcone A, a new antimalarial agent, inhibits in vitro growth of the human malaria parasite *Plasmodium falciparum* and protects mice from *P. yoelii* infection. Antimicrob Agents Chemother. 1994;38:1470–5.
29. Ariefta NR, Pagmadulam B, Hatano M, Ikeda N, Isshiki K, Matoba K, et al. Antiplasmodial activity evaluation of a bestatin-related aminopeptidase inhibitor, phebestin. Antimicrob Agents Chemother. 2023;67:e010622.
30. Edgar RCS, Siddiqui G, Hjerrild K, Malcolm TR, Vinh NB, Webb CT, et al. Genetic and chemical validation of *Plasmodium falciparum* aminopeptidase PfA-M17 as a drug target in the hemoglobin digestion pathway. Elife. 2022;11:e80813.
31. Aguado ME, Izquierdo M, González-Matos M, Varela AC, Méndez Y, del Rivero MA, et al. Parasite metalo-aminopeptidases as targets in human infectious diseases. Curr Drug Targets. 2023;24:416–61.
32. Lee AH, Dhingra SK, Lewis IA, Singh MK, Siriwardana A, Dalal S, et al. Evidence for regulation of hemoglobin metabolism and intracellular ionic flux by the *Plasmodium falciparum* chloroquine resistance transporter. Sci Rep. 2018;8:13578.
33. Okombo J, Mok S, Qahash T, Yeo T, Bath J, Orchard LM, et al. Piperaquine-resistant PfCRT mutations differentially impact drug transport, hemoglobin catabolism and parasite physiology in *Plasmodium falciparum* asexual blood stages. PLoS Pathog. 2022;18:e1010926.
34. Melzig M, Bormann H. Betulinic acid inhibits aminopeptidase N activity. Planta Med. 1998;64:655–7.
35. Mahanta PJ, Lhouvum K. *Plasmodium falciparum* proteases as new drug targets with special focus on metalloproteases. Mol Biochem Parasitol. 2024;258:111617.
36. Giannangelo C, Challis MP, Siddiqui G, Edgar R, Malcolm TR, Webb CT, et al. Chemoproteomics validates selective targeting of *Plasmodium* M1 alanyl aminopeptidase as an antimalarial strategy. Elife . 2024 J;13:1–32.
37. Vinh NB, Drinkwater N, Malcolm TR, Kassiou M, Lucantoni L, Grin PM, et al. Hydroxamic acid inhibitors provide cross-species inhibition of *Plasmodium* M1 and M17 Aminopeptidases. J Med Chem. 2019;62:622–40.
38. Malcolm TR, Swiderska KW, Hayes BK, Webb CT, Drag M, Drinkwater N, et al. Mapping the substrate specificity of the *Plasmodium* M1 and M17 aminopeptidases. Biochem J. 2021;478:2697–713.
39. Mathew R, Wunderlich J, Thivierge K, Cwiklinski K, Dumont C, Tilley L, et al. Biochemical and cellular characterisation of the *Plasmodium falciparum* M1 alanyl aminopeptidase (PfM1AAP) and M17 leucyl aminopeptidase (PfM17LAP). Sci Rep. 2021;11:2854.
40. McGowan S, Oellig CA, Birru WA, Caradoc-Davies TT, Stack CM, Lowther J, et al. Structure of the *Plasmodium falciparum* M17 aminopeptidase and significance for the design of drugs targeting the neutral exopeptidases. Proc Natl Acad Sci U S A. 2010;107:2449–54.
41. WHO. Traditional Medicine Strategy 2014–2023. Geneva, World Health Organization, 2013;1–76. http://apps.who.int/iris/bitstream/10665/92455/1/9789241506090_eng.pdf?ua=1 (Accessed 09.09.2016)
42. Atanasov AG, Zotchev SB, Dirsch VM, Orhan IE, Banach M, Rollinger JM, et al. Natural products in drug discovery: advances and opportunities. Nat Rev Drug Discov. 2021;20:200–16.
43. Sleebs BE, Lopaticki S, Marapana DS, O'Neill MT, Rajasekaran P, Gazdik M, et al. Inhibition of plasmepsin V activity demonstrates its essential role in protein export, PfEMP1 display, and survival of malaria parasites. PLoS Biol. 2014;12:e1001897.
44. Boonyalai N, Collins CR, Hackett F, Withers-Martinez C, Blackman MJ. Essentiality of *Plasmodium falciparum* plasmepsin V. PLoS ONE. 2018;13:e027621.
45. Poreba M, McGowan S, Skinner-Adams TS, Trenholme KR, Gardiner DL, Whisstock JC, et al. Fingerprinting the substrate specificity of M1 and M17 aminopeptidases of human malaria, *Plasmodium falciparum*. PLoS ONE. 2012;7:e31938.
46. Allary M, Schrevel J, Florent I. Properties, stage-dependent expression and localization of *Plasmodium falciparum* M1 family zinc-aminopeptidase. Parasitology. 2002;125:1–10.
47. Jacobsen JA, Fullagar JL, Miller MT, Cohen SM. Identifying chelators for metalloprotein inhibitors using a fragment-based approach. J Med Chem. 2011;54:591–602.
48. da Silva GN, Maria NRG, Schuck DC, Cruz LN, de Moraes MS, Nakabashi M, et al. Two series of new semisynthetic triterpene derivatives: differences in anti-malarial activity, cytotoxicity and mechanism of action. Malar J. 2013;12:89.
49. Suksamrarn A, Tanachatchairatana T, Kanokmedhakul S. Antiplasmodial triterpenes from twigs of *Gardenia saxatilis*. J Ethnopharmacol. 2003;88:275–7.
50. Suksamrarn S, Panseeta P, Kunchanawatta S, Distaporn T, Ruktasing S, Suksamrarn A. Ceanothane- and lupane-type triterpenes with antiplasmodial and antimycobacterial activities from *Ziziphus cambodiana*. Chem Pharm Bull. 2006;54(4):535–7.

Publisher's Note